EPJ Web of Conferences **353**, 01011 (2026) https://doi.org/10.1051/epjconf/202635301011
mm Universe 2025

The SZ-Mass scaling relation with the NIKA2 SZ Large Program

A. Moyer-Anin[1], R. Adam[2], P. Ade[3], H. Ajeddig[4], S. Amarantidis[6], P. André[4], H. Aussel[4], I. Bartalucci[5], A. Beelen[7], A. Benoît[8], S. Berta[9], M. Béthermin[10], B. Bolliet[11], A. Bongiovanni[6], J. Bounmy[1], O. Bourrion[1], M. Calvo[8], A. Catalano[1], D. Chérouvrier[1], M. De Petris[12], F.-X. Désert[13], S. Doyle[3], E. F. C. Driessen[9], G. Ejlali[14], A. Ferragamo[12], A. Gomez[15], J. Goupy[8], C. Hanser[16], S. Katsioli[17,18], F. Kéruzoré[19], C. Kramer[9], B. Ladjelate[6], G. Lagache[7], S. Leclercq[9], J.-F. Lestrade[20], J. F. Macías-Pérez[1], S. C. Madden[4], A. Maury[21,22,4], F. Mayet[1], J.B. Melin[23], A. Monfardini[8], M. Muñoz-Echeverría[24], I. Myserlis[6], A. Paliwal[25], L. Perotto[1], G. Pisano[12], E. Pointecouteau[24], N. Ponthieu[13], G. W. Pratt[4], V. Revéret[4], A. J. Rigby[26], A. Ritacco[1], H. Roussel[27], F. Ruppin[28], M. Sánchez-Portal[6], S. Savorgnano[1], K. Schuster[9], A. Sievers[6], C. Tucker[3], R. Wicker[12], and G. Yepes[29]

[1]Univ. Grenoble Alpes, CNRS, LPSC-IN2P3, 53, av. des Martyrs, 38000 Grenoble, France
[2]Université Côte d'Azur, Observatoire de la Côte d'Azur, CNRS, Laboratoire Lagrange, France
[3]School of Physics and Astronomy, Cardiff University, Queen's Buildings, The Parade, Cardiff, CF24 3AA, UK
[4]Université Paris Cité, Université Paris-Saclay, CEA, CNRS, AIM, F-91191 Gif-sur-Yvette, France
[5]INAF, IASF-Milano, Via A. Corti 12, 20133 Milano, Italy.
[6]Institut de Radioastronomie Millimétrique (IRAM), Avenida Divina Pastora 7, Local 20, E-18012, Granada, Spain
[7]Aix Marseille Univ, CNRS, CNES, LAM (Laboratoire d'Astrophysique de Marseille), Marseille, France
[8]Institut Néel, CNRS, Université Grenoble Alpes, France
[9]Institut de RadioAstronomie Millimétrique (IRAM), Grenoble, France
[10]Université de Strasbourg, CNRS, Observatoire astronomique de Strasbourg, UMR 7550, 67000 Strasbourg, France
[11]DAMTP, Centre for Mathematical Sciences, Wilberforce Road, Cambridge CB3 0WA, U.K.
[12]Dipartimento di Fisica, Sapienza Università di Roma, Piazzale Aldo Moro 5, I-00185 Roma, Italy
[13]Univ. Grenoble Alpes, CNRS, IPAG, 38000 Grenoble, France
[14]Institute for Research in Fundamental Sciences (IPM), School of Astronomy, Tehran, Iran
[15]Centro de Astrobiología (CSIC-INTA), Torrejón de Ardoz, 28850 Madrid, Spain
[16]Aix Marseille Univ, CNRS/IN2P3, CPPM, Marseille, France
[17]National Observatory of Athens, Institute for Astronomy, Astrophysics, Space Applications and Remote Sensing, Ioannou Metaxa and Vasileos Pavlou GR-15236, Athens, Greece
[18]Department of Astrophysics, Astronomy & Mechanics, Faculty of Physics, University of Athens, Panepistimiopolis, GR-15784 Zografos, Athens, Greece
[19]High Energy Physics Division, Argonne National Laboratory, 9700 South Cass Av., Lemont, IL 60439, USA
[20]LERMA, Observatoire de Paris, PSL Research University, CNRS, Sorbonne Université, UPMC, 75014 Paris, France
[21]Institute of Space Sciences (ICE), CSIC, Campus UAB, Carrer de Can Magrans s/n, E-08193, Barcelona, Spain
[22]ICREA, Pg. Lluís Companys 23, Barcelona, Spain

[23]Université Paris-Saclay, CEA, Département de Physique des Particules, 91191 Gif-sur-Yvette, France

[24]IRAP, CNRS, Université de Toulouse, CNES, UT3-UPS, (Toulouse), France
[25]Dipartimento di Fisica, Università di Roma 'Tor Vergata', Via della Ricerca Scientifica 1, I-00133 Roma, Italy
[26]School of Physics and Astronomy, University of Leeds, Leeds LS2 9JT, UK
[27]Institut d'Astrophysique de Paris, CNRS (UMR7095), 98 bis boulevard Arago, 75014 Paris, France
[28]University of Lyon, UCB Lyon 1, CNRS/IN2P3, IP2I, 69622 Villeurbanne, France
[29]Departamento de Física Teórica and CIAFF, Facultad de Ciencias, Univ. Autónoma de Madrid, 28049 Madrid, Spain.

Abstract. In Sunyaev-Zeldovich (SZ) cluster cosmology, accurately determining cluster masses is crucial for constraining cosmological parameters through cluster number counts. As the mass is not an observable, a scaling relation is needed to link cluster masses to the integrated Compton parameter Y, i.e., the SZ observable, to exploit data from large millimeter surveys. Former cosmological results use a scaling relation obtained with clusters at low redshift ($z < 0.5$) observed in X-ray and in SZ at an angular resolution above 1 arcminute. The SZ large program (LPSZ) of the NIKA2 collaboration uses a sample of clusters at intermediate to high redshift (from $z = 0.5$ to $z = 0.9$) observed at similarly high-angular resolution both in SZ and in X-ray. We present the SZ-Mass scaling relation parameters calibrated thanks to the LPSZ data.

1 Introduction

Galaxy clusters are formed at the densest peaks in the matter density field. They are thus ideal probes to constrain cosmological parameters. They can be observed at several wavelengths to study their different components. The intra-cluster medium (ICM) can be studied thanks to millimeter observations through the thermal Sunyaev-Zeldovich (tSZ) effect [1]. It is an inverse Compton scattering of the Cosmic Microwave Background (CMB) photons by the cluster ionized gas. This effect distorts the CMB spectrum towards higher frequencies and its amplitude is quantified by the Compton-y parameter that is proportional to the integral of the electron pressure $P_e(r)$ of the ICM along the line of sight. We define the integrated SZ observable Y_{500} as the surface integrated Compton-y parameter. Several large scale surveys, such as Planck [2], ACT [3] and SPT [4], have constructed SZ-detected cluster catalogs used to constrain cosmological parameters with cluster number counts [5]. Cluster masses are thus a key quantity for cosmology, but unfortunately they are not a direct observable. For this reason, we need a scaling relation linking the SZ observable Y_{500} to $M_{500}^{\rm HSE}$. We define $M_{500}^{\rm HSE}$ as the mass within a sphere with an average density 500 times the critical density of the Universe and in hydrostatic equilibrium. It is derived from the combination of the SZ pressure profile $P_e(r)$ and the X-ray electron density profile $n_e(r)$: $M_{\rm HSE}(< r) = -r^2/(Gmn_e(r)) \times {\rm dP_e(r)/dr}$ with G the gravitational constant and m the ICM mean molecular mass.

2 The Y_{500}-$M_{500}^{\rm HSE}$ scaling relation

The Y_{500}-M_{500} relation is derived assuming spherical symmetry and hydrostatic equilibrium. It is expressed as a power law relation [6]:

$$E_z^{-2/3}\left(\frac{D_A^2 Y_{500}}{10^{-4}{\rm Mpc}^2}\right) = 10^{\alpha}\left(\frac{(1-b)M_{500}^{\rm tot}}{6\times10^{14}{\rm M}_\odot}\right)^{\beta} \quad (1)$$

where b is the hydrostatic bias, $E_z = H(z)/H_0$ and D_A the angular diameter distance.
However, the previous assumptions do not describe the full variety of clusters in the Universe. Therefore, the scaling relation is modeled as a Gaussian distribution with mean defined in equation (1) and intrinsic dispersion σ_{int}:

$$P(\log(\widetilde{Y}_{500})|\log(\widetilde{M}_{500}^{\rm HSE})) = \mathcal{N}(\alpha + \beta\log(\widetilde{M}_{500}^{\rm HSE}), \sigma_{int}^2) \quad (2)$$

where $\widetilde{Y}_{500}$ corresponds to the left-hand side of equation (1) and $\widetilde{M}_{500}^{\rm HSE}$ is equal to the term in brackets on the right-hand side.
Hence, the scaling relation is defined by three parameters: α the intercept, β the slope and σ_{int} the intrinsic scatter. Previous estimations of these parameters are presented in [6, 7]. The mentioned works used low-redshift clusters ($z \leq 0.45$) and SZ data with low angular resolution (~ 6 arcmin), thus, their mass estimates rely purely on X-ray observations.
The SZ Large Program (LPSZ) [8] of the NIKA2 collaboration provides mass estimates combining X-ray and SZ observations thanks to the high-angular resolution NIKA2 camera [9]. It is installed at the IRAM 30-m telescope near Granada and observes at 150 and 260 GHz with high angular resolutions of 17.6" and 6.6" respectively [10, 11]. The observation of the SZ decrement at 150 GHz allows us to obtain a robust estimate of Y_{500}. In this work, we use 29 clusters from the LPSZ sample at intermediate to high redshift ($z \in [0.5, 0.9]$) selected from the Planck and ACT surveys using 2D bins in mass (5 bins) and redshift (2 bins) referred to as the box selection function. The aim of this selection was to avoid the effect of the non-uniform underlying mass distribution and in order to assure uniform coverage across mass and redshift. However, properly accounting for this box selection function in further analyses is not trivial, since there are 5 thresholds along the mass axes that can not be treated individually, which is difficult to account for in a likelihood function. The LPSZ sample in the Y_{500}-redshift plane is presented in figure 1. The boxes used for the selection are plotted in black and the Y_{500} LPSZ estimations are plotted in dark circles with their corresponding error bars. Note that the Y_{500} values are the ones measured by NIKA2 and they can differ from the initial Planck or ACT estimates, which results in the reorganization of clusters within the 2D bins. The red boxes correspond to the final sample with two additional boxes at low mass to match the LPSZ Y_{500} estimates.

3 LIRA+SBI pipeline

To account for the complex and specific LPSZ selection function, we developed a 2-stage pipeline that combines the LIRA software (LInear Regression in Astronomy) [12] with a Simulation Based Inference (SBI) method [13]. LIRA provides a reliable estimation of the scaling relation parameters while taking into account the uncertainties and correlation of each cluster in the sample. SBI is a likelihood-free inference method based on normalizing flows used when the likelihood is complex and computationally expensive to be expressed analytically. LIRA is used as a first step to reduce the size of the parameter space to only the scaling relation parameters, making the SBI analysis more efficient and focused solely on the impact of the LPSZ selection function. The LIRA+SBI pipeline is summarized in figure 2. Here, "Sample simulation" refers to an analytical simulation generating an LPSZ-like sample, which consists of a set of Y_{500}, M_{500} and z. These values are generated using an input scaling relation, the Tinker mass function [14], and the error and correlation distributions of the LPSZ data. For each simulated sample, LIRA provides an estimation of the scaling relation parameters affected by the selection function. The SBI method is then trained to correct for the impact of the box selection function with input and recovered scaling relations.

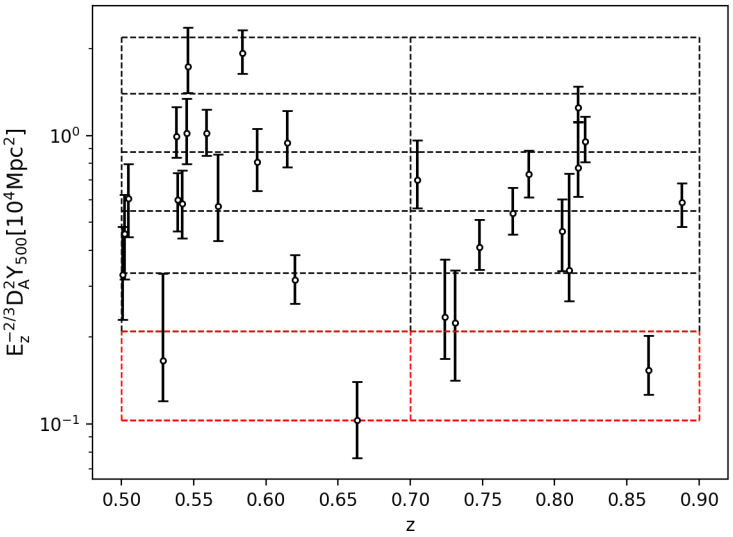

Figure 1. Distribution of the LPSZ sample in the Y_{500}–redshift plane. Black boxes show the original selection, red boxes represent the updated boxes following LPSZ observations.

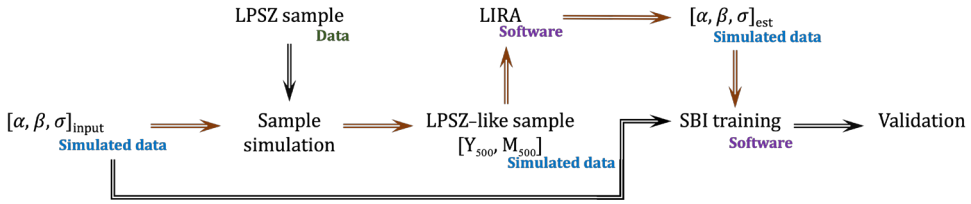

Figure 2. Overview of the LIRA+SBI pipeline. LPSZ-like samples are analytically generated and regressed with LIRA, then used to train the SBI method with the input scaling relation to account for the LPSZ selection function.

4 Validation and results

Before applying the LIRA+SBI pipeline to the LPSZ sample, we need to verify that the selection function is correctly taken into account. The primary metric is obtained from studying the distribution of the recovered parameter bias: $bias_{std} = (X_{true} - X_{est})/\Delta_{X_{est}}$, where X_{true} are the input parameters, and $[X_{est}, \Delta_{X_{est}}]$ their estimated values and uncertainties. If the obtained posterior is unbiased and with coherent error bars, the $bias_{std}$ distribution should follow a Gaussian distribution with mean 0 and standard deviation 1. This test for the final LPSZ sample is presented in figure 3 where the distributions of the $bias_{std}$ for the scaling relation parameters are plotted with the expected Gaussian distributions. This test, along with TARP diagnostic [15], validates the training of the LIRA+SBI pipeline. We can then apply it to the LPSZ data. The results are summarized in table 1 along with previous estimates of the SZ-mass scaling relation. The uncertainties we obtain are larger, which is partially explained by the size of our sample and the fact that our mass estimations are independent from a T_X-

mass scaling relation. The slope β is significantly lower suggesting a redshift evolution. This evolution, also observed in [16] with simulations, could be explained by the evolution of the non-thermal pressure fraction, which increases more strongly with redshift in the most massive clusters.

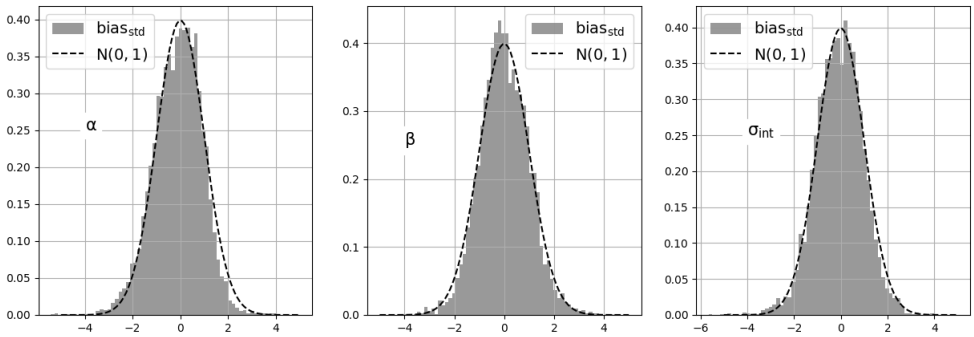

Figure 3. Histograms of the $bias_{std}$ for the three scaling relation parameters compared to the expected Gaussian distribution plotted as the dotted line.

The figure 4 shows the LPSZ sample in the $\widetilde{Y}_{500} - \widetilde{M}^{\rm HSE}_{500}$ plane together with our scaling relation calibration in blue, compared to the previous estimation at low redshift. Our slope is in tension with previous estimations. However, the agreement between LPSZ data and the fitted model is satisfactory.

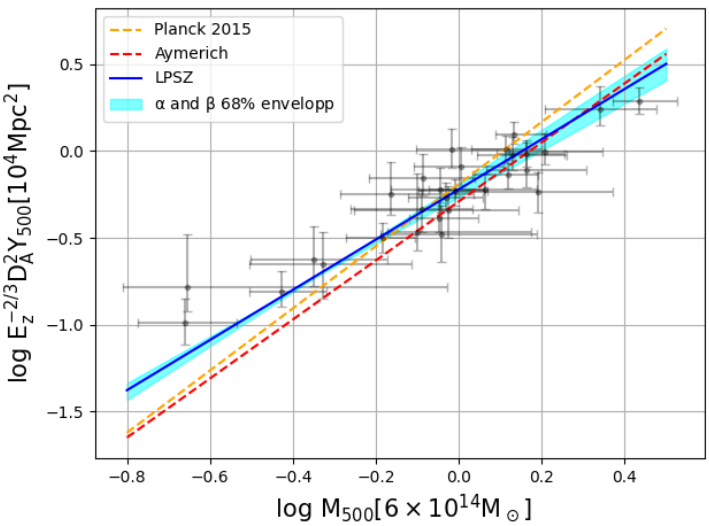

Figure 4. LPSZ sample in black plotted with the LPSZ scaling relation (blue line) with its uncertainty (blue envelope). The Planck [6] and Chandra-Planck [7] scaling relations are respectively plotted in orange and red.

	α	β	σ_{int}	redshift range	sample size
Planck	-0.19 ± 0.02	1.79 ± 0.08	0.075 ± 0.01	[0 - 0.45]	71
Chandra-Planck	-0.29 ± 0.01	1.70 ± 0.1	0.083 ± 0.01	[0 - 0.35]	146
LPSZ	-0.22 ± 0.04	1.45 ± 0.12	0.068 ± 0.29	[0.5 - 0.9]	29

Table 1. Estimation of the scaling relation parameters for Planck [6] and Chandra-Planck [7] compared to the LPSZ estimation presented in this proceeding.

5 Conclusion

We presented the LIRA+SBI pipeline developed to deliver a robust and reliable scaling relation estimation while accounting for the specific LPSZ selection function. Applied to the LPSZ sample, it results in a new scaling relation estimation at high redshift, suggesting a redshift evolution of the slope β. Thanks to this result, we will be able to update cosmological constraints from previous surveys by applying a scaling relation corresponding to the relevant redshift range [17]. More detailed papers and a complete analysis of the LPSZ presenting the final results are expected to be published by the end of the year 2025.

Acknowledgements

We would like to thank the IRAM staff for their support during the observation campaigns. The NIKA2 dilution cryostat has been designed and built at the Institut Néel. In particular, we acknowledge the crucial contribution of the Cryogenics Group, and in particular Gregory Garde, Henri Rodenas, Jean-Paul Leggeri, Philippe Camus. This work has been partially funded by the Foundation Nanoscience Grenoble and the LabEx FOCUS ANR-11-LABX-0013. This work is supported by the French National Research Agency under the contracts "MKIDS", "NIKA" and ANR-15-CE31-0017 and in the framework of the "Investissements d'avenir" program (ANR-15-IDEX-02). This work has been supported by the GIS KIDs. This work has benefited from the support of the European Research Council Advanced Grant ORISTARS under the European Union's Seventh Framework Programme (Grant agreement No. 291294). R. A. acknowledges support from the Programme National Cosmology et Galaxies (PNCG) of CNRS/INSU with INP and IN2P3, co-funded by CEA and CNES. R. A. was supported by the French government through the France 2030 investment plan managed by the National Research Agency (ANR), as part of the Initiative of Excellence of Université Côte d'Azur under reference number ANR-15-IDEX-01. A. Maury acknowledges support the funding from the European Research Council (ERC) under the European Union's Horizon 2020 research and innovation programme (Grant agreement No. 101098309 - PEBBLES). M.M.E. acknowledges the support of the French Agence Nationale de la Recherche (ANR), under grant ANR-22-CE31- 0010.

References

[1] R. A. Sunyaev & Y. B. Zeldovich, Astro. and Space Science **7**,20 (1970)
[2] Planck Collaboration *et al.*, Astron. Astrophys. **594**, A27 (2016)
[3] M. Hilton *et al.*, American Astronomical Society, **253**,3 (2021)
[4] L.E. Bleem *et al.*, ApJS **247**,25 (2020)
[5] A. Vikhlinin *et al.*, The Astrophysical Journal, **692**, 1060 (2009)
[6] Planck Collaboration *et al.*, Astron. Astrophys., **571**, A20 (2014)
[7] G. Aymerich *et al.*, Astron. Astrophys., **690**, A238 (2024)
[8] F. Mayet *et al.*, EPJ Web of Conferences **228**, 00017 (2020)
[9] L. Perotto *et al.*, Astron. Astrophys. **637**, A71 (2020)
[10] R. Adam *et al.*, Astron. Astrophys. **609**, A115 (2018)
[11] M. Calvo *et al.*, Journal of Low Temperature Physics, **184**, 816 (2016)
[12] M. Sereno, MNRAS **455**, 2149 (2016)
[13] A. Tejero-Cantero *et al.*, JOSS, **5**, 2505 (2020)
[14] J. Tinker *et al.*, The Astrophysical Journal **688**, 710 (2008)
[15] P. Lemos *et al.*, arXiv:2302.03026
[16] S. B. Green *et al.*, MNRAS **496**, 2743 (2020)
[17] A. Moyer-Anin *et al.*, in prep